High-field Zeeman and Paschen-Back effects at high pressure in oriented ruby

Marius Millot and Jean-Marc Broto*
Laboratoire National des Champs Magnétiques Pulsés (LNCMP), Université de Toulouse, 143 avenue de Rangueil, 31400 Toulouse, France

Jesus Gonzalez†
DCITIMAC-Malta Consolider Team, Universidad de Cantabria, Avenida Los Castros S/N, 39005 Santander, Cantabria, Spain
(Received 25 August 2008; published 28 October 2008)

High-field Zeeman and Paschen-Back effects have been observed in single crystals of ruby submitted to hydrostatic pressure up to 10 GPa. A specific setup with a miniature diamond-anvil cell has been developed to combine high pressure and pulsed magnetic fields and to perform magnetophotoluminescence measurements. Careful analysis of low-temperature (4.2 and 77 K) photoluminescence spectra with a 56 T magnetic field applied along the *c* axis allows for the rectification of the assignment of observed emission lines to corresponding Zeeman-split levels. Besides, the intrinsic Zeeman-splitting factors of excited states reveal a linear pressure-induced increase. This enhancement is a signature of an increase in trigonal distortion induced by hydrostatic pressure. Moreover, spectra with magnetic field perpendicular to crystallographic *c* axis exhibit a Paschen-Back effect reflecting the progressive alignment of Cr^{3+} ions spin along the applied field. However, no pressure modification is observed in this compound, contrarily to the Heisenberg-to-Ising spin character pressure-induced transition observed in alexandrite.

DOI: 10.1103/PhysRevB.78.155125 PACS number(s): 78.20.Ls, 78.55.Hx

I. INTRODUCTION

Up to now, only a few experiments have been carried out combining both high pressure and high magnetic fields. However, some fruitful studies on semiconductors, organic conductors, high-T_c superconductors, and carbon nanotubes have stimulated the development of new apparatus going beyond current frontiers.[1–4] Most of these studies are either using diamond-anvil cells (DACs) up to 10 GPa in magnetic fields below 45 T (Ref. 5) or large-volume anvil cells below 1.5 GPa in 60 T magnets.[6] We report here on some magnetophotoluminescence studies on oriented ruby in pulsed magnetic field up to 60 T under high pressure up to 10 GPa. Our setup allows an extension of the experimentally achievable extreme conditions for both optical [photoluminescence (PL) and absorption] and electronic transport measurements and opens the way to coupled measurements such as electroluminescence or photoconductivity. Some adjustments have been made possible in the assignation of observed emission lines with corresponding electronic transition between Zeeman degeneracy lifted levels. In addition, evidences of an enhancement of the trigonal distortion induced by the pressure in hydrostatic conditions are detailed. We briefly review hereinafter the electronic and structural properties of ruby then we describe in details our experimental setup in Sec. II. Results are presented and discussed in Sec. III. Under magnetic field, a splitting of *R* lines is observed. As it appears to depend on the direction of the applied field with respect to *c* axis, we will first focus on results with magnetic field along trigonal axis. Then we will describe and analyze the perpendicular configuration. Finally, in Sec. III B a precise analysis of the evolution under high pressure of the microscopic parameters involved in the magnetic behavior is presented.

Optical properties of ruby have been extensively studied in the last decades owing to solid-state laser applications of this well-known red gemstone. Ruby is a chromium-doped form of corundum Al_2O_3 with Cr^{3+} substituted for aluminum ions. Ruby crystallizes in a close-packed hexagonal structure slightly distorted by repulsion between neighboring cations. Although the symmetry is reduced from cubic O_h to trigonal C_3.[7,8] Ligand-field approach is quite reliable to describe electronic properties of ruby with low Cr^{3+} concentration. Assuming in first approximation a cubic field on the three *d* electrons of the Cr^{3+} ions, one can easily obtain electronic level diagrams by treating both trigonal distortion (V_{tr}) and spin-orbit interaction (H_{SO}) as perturbations. The first-excited cubic state ^2E is split by the interplay of both perturbations resulting in two Kramers' doublet $\bar{E}$ and $2\bar{A}$.[9] These two degenerated states are, respectively, responsible for intense and narrow emission lines R_1 and R_2 around 694 nm at ambient conditions. The $^4A_2$ ground-state spin value is 3/2. A third-order interaction gives rise to a zero-field splitting $\delta = 0.38$ cm^{-1} between $\pm 1/2$ and $\pm 3/2$ levels.[10] However, due to the very small value of δ this lift of degeneracy is generally not directly observable. The R_1 and R_2 lines are routinely used as *in situ* pressure[11,12] and temperature sensors[13] in transparent high-pressure devices.

II. EXPERIMENTAL SETUP

Measurements have been carried out under pulsed magnetic fields at the Laboratoire National des Champs Magnétiques Pulsés (LNCMP) in Toulouse. Nondestructive 3 MJ coil connected to a 14 MJ capacitor bank can produce 60 T every hour; thanks to liquid-nitrogen fast-cooling system. The time profile of one magnetic shot is exhibited in Fig. 1 as measured by integration of the inductive voltage in a pickup coil. The long duration of the pulse with 250 ms exponential decay owing to crowbar resistance allows performing optical experiments even with millisecond range accumulation time. By tuning the capacitor bank voltage we

 ©2008 The American Physical Society

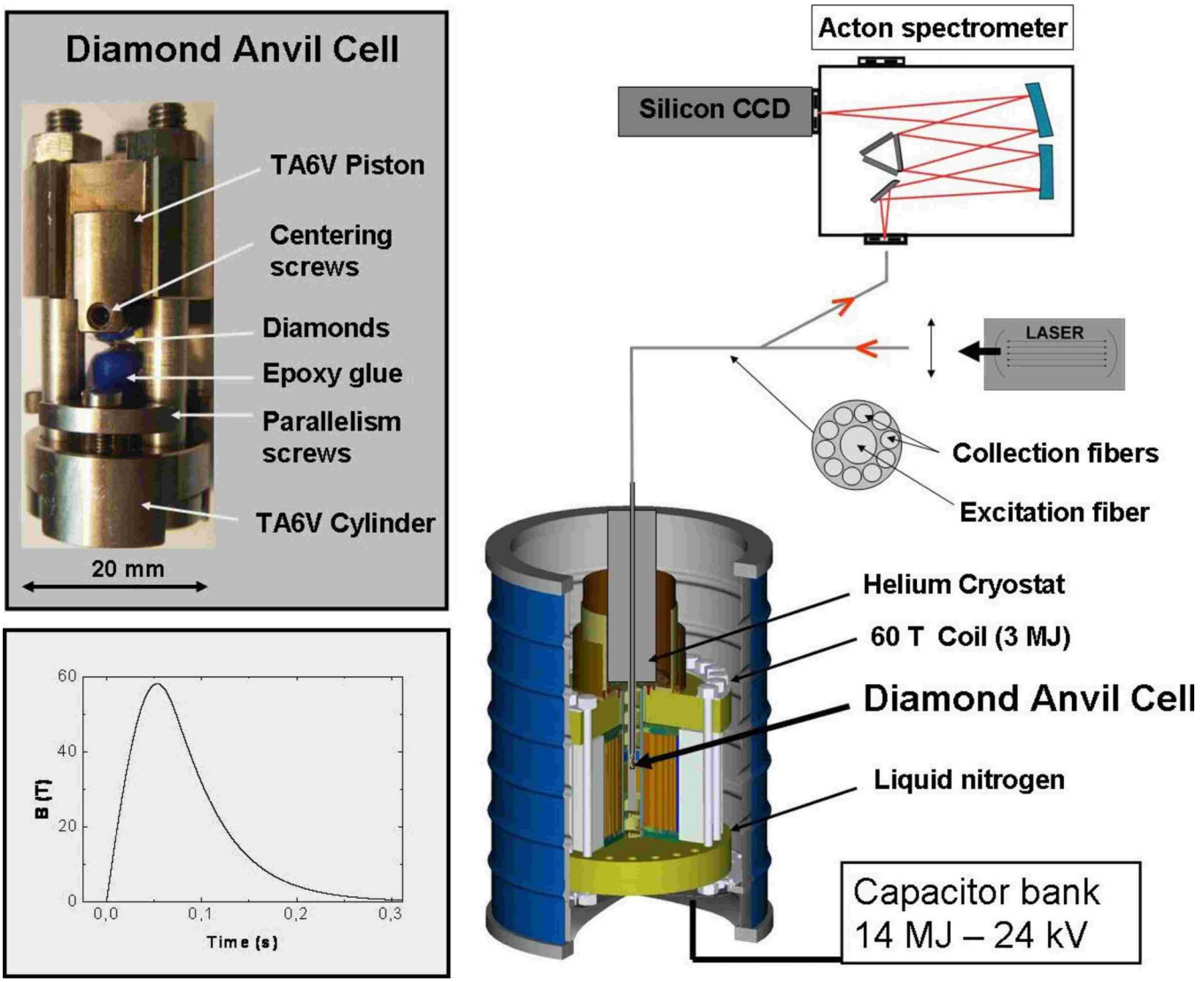

FIG. 1. (Color online) Experimental setup of magnetophotoluminescence under high hydrostatic pressure using a DAC. The upper left inset shows the miniature pressure cell designed for pulsed magnetic-field environment. The time profile of one magnetic experiment is plotted below.

can adjust the maximum value of each field pulse. The narrow inner diameter of the helium bath cryostat inserted in the 26 mm coil bore, together with the induction of large eddy currents in any conductive part of the setup submitted to the pulsed magnetic field, has led us to design a specific miniature DAC to generate high pressure in the heart of the pulsed magnet. We have selected the nonmagnetic titanium-based TA6V alloy for its mechanical, electrical, and magnetic properties. The DAC diameter of 20 mm and the double beveled diamonds with 700 μm culets allow submitting samples of $150\times150\times30$ μm^3 at quasihydrostatic pressure up to 10 GPa. Pressure is generated at room temperature using a hydraulic press in conjunction with a force sensor. Inconel 718 gasket and liquid pressure transmitting medium such as 4:1 methanol-ethanol mixture are used.[14] For *in situ* pressure measurements at low temperature and also magnetophotoluminescence experiments a tailor-made optical fiber bundle has been designed (Fig. 1). The Faraday configuration is permanently used. Laser excitation is injected into a 200-μm-diameter silicon oxide fiber illuminating the back side of the diamond anvil, whereas ten 100-μm-diameter fibers are used to collect photoluminescence light and drive it to the entrance slit of a 0.3 m triple grating Acton spectrometer with 1340×100 pixel silicon CCD detector sensitive from 500 to 900 nm with a resolution [full width at half maximum (FWHM)] of 0.12 nm. The acquisition time varies from 1 to 10 ms, depending on the luminescence intensity. A numerical optical pretrigger system allows precise synchronization between field pulse maximum plateau and optical acquisition ensuring field variation during a spectrum acquisition at this maximum value of the field pulse with $\Delta B/B$ better than 0.1%. In addition, our fast acquisition technique enables also to produce up to 50 spectra at different magnetic-field values during the pulsed magnetic-field decay with $\Delta B/B$ values of roughly 1% with a 5 ms accumulation time.

The samples are ruby single crystals containing 4000 ppm of chromium. They have been optically oriented either along

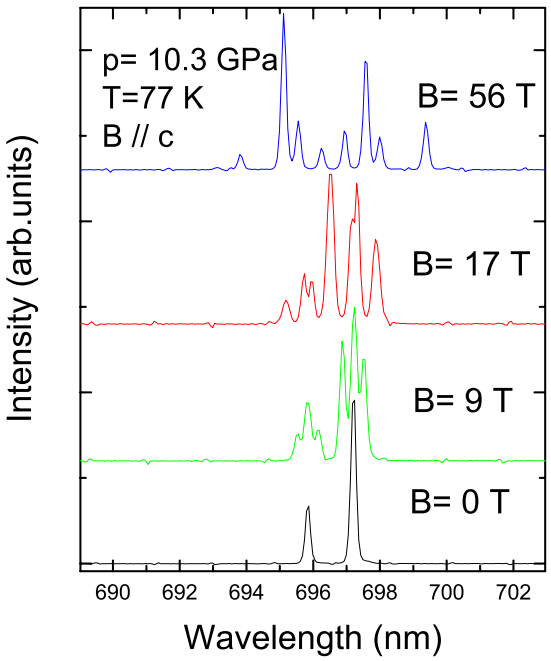

FIG. 2. (Color online) Evolution of ruby R lines PL spectrum with increasing magnetic field. The pressure is 10.3 GPa and the magnetic field is applied along the c axis in Faraday configuration.

and perpendicular to the trigonal c axis and mechanically polished down to a 20 μm thickness.

III. RESULTS AND DISCUSSION

We have performed several cycles of pressure experiments with different samples of both orientations up to 10 GPa at liquid-nitrogen and liquid-helium temperatures. The spectral analysis of PL is focused on R_1 and R_2 lines around 694 nm. Pressure-induced redshift of R_1 peak is used as *in situ* pressure sensor assuming a 0.365 nm GPa^{-1} variation at room temperature[11,12] and a temperature-induced blueshift between 108 and 300 K well described by quadratic dependence tabulated in Ref. 15 ensuring 0.1 GPa precision in pressure determination. Furthermore, considering the very weak intensity of the ion-pair emission lines and the low concentration of chromium ions (4000 ppm), we will neglect in the following any effect related to interactions between neighbor Cr^{3+} ions.[16]

A. Magnetic effects on PL spectra

1. Magnetic field applied along the c axis

The lift of degeneracy induced by magnetic field of R lines at 77 K is shown on Fig. 2 recorded at 10.3 GPa. Up to 9 T both R lines split in only three distinct peaks, which is in qualitative agreement with low-field previous works at ambient[7,8] and high pressures.[1] However, above 17 T one can notice that the central peak is divided in two. Finally, eight PL lines are clearly distinguishable. Using the spectra recorded at different values of the applied magnetic field for each pressure, one can easily follow the evolution of each peak up to 60 T and determine, through a multi-Gaussian deconvolution analysis, the splitting pattern exhibited in Fig. 3. Therefore, a fourfold lift of degeneracy of both R lines appears clearly and the peak energies' evolution turns out to be linear with the applied field. We expect a linear Zeeman effect with an energy shift described by the well-known formula

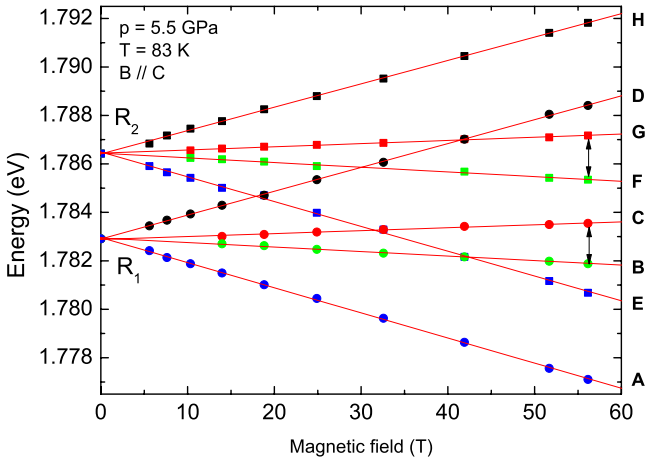

FIG. 3. (Color online) Zeeman-splitting pattern of ruby R lines recorded at high pressure (5.5 GPa) with B along the c axis. Experimental peak positions (symbols) are extracted from spectra recorded at different magnetic-field values after multi-Gaussian fits. A very good agreement is achieved with Zeeman effect linear behavior (solid lines). Arrows indicate excited states splitting directly resolved in the present experiment at all pressures; thanks to the 55 T applied field.

$$\Delta E = m_s g \mu_B B, \tag{1}$$

where m_s is the magnetic quantum number, g is the so-called Zeeman factor, μ_B is the Bohr magneton, and B is the magnetic field applied along quantization direction, i.e., here the c axis. In the easiest case, assuming identical splitting for, on one hand, the ground state and both excited states on the other hand, one should expect a perfect symmetrical pattern for magnetic shifts. However, one can easily notice that even for the highest-energy peak of each R line, labeled as D and H, or for the lowest-energy peaks (A,E) the observed slope differs dramatically. In addition, the energy gap between the two central peaks (B,C) and (F,G) of respective R_1 and R_2 patterns indicated by arrows on Fig. 3 is also clearly different.

We have subsequently analyzed in details the structure of spectra at maximum field for each pressure. Figure 4 shows an example of spectrum at maximum field at 1.5 GPa and 56 T. Thanks to this careful analysis, we were able to assign all R_1 and R_2 emission lines with corresponding electronic transitions as shown in Figs. 4 and 5. With the help of extensive calculations by Sugano *et al.*[7,8] and taking into account the selection rules in our experimental configuration $(B\|c, E\perp c)$, we can distinguish eight major peaks corresponding to the eight allowed dipolar transitions. Besides, four weaker peaks are observed which are allowed with $E\|c$. The energy differences between all those transitions are indicated in Fig. 4 in $\mu_B B$ units and are consistent with results

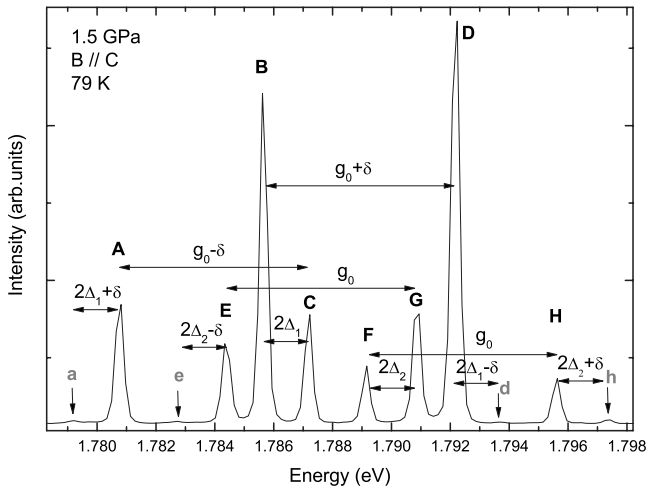

FIG. 4. Spectrum of R lines Zeeman pattern at maximum field (56 T) recorded at 1.5 GPa and 79 K. Eight major ($A-H$) and four weaker ($a-h$) peaks are clearly distinguishable and energy differences between them are labeled on arrows in $\mu_B B$ units.

in the complementary configuration ($B \perp c$) discussed in Sec. III A 2. Four parameters are needed to describe the Zeeman pattern: g_0, the ground-state Zeeman factor; δ, the zero-field splitting between 3/2 and 1/2 ground states; and Δ_1 and Δ_2, the intrinsic excited states splitting factors. Effective splitting of excited states is, respectively, $g_0+2\Delta_1$ and $g_0-2\Delta_2$ as indicated in Fig. 5. The low-temperature (4 K) spectrum at maximum field presented in Fig. 6 exhibits only two major peaks and a weak one. By the superposition of liquid-nitrogen and liquid-helium temperature spectra the assignation of these three peaks is evidenced. Thus, assuming that at this low temperature the only excited level populated is the lowest one $(\bar{E},-1/2)$ we can assume with confidence that

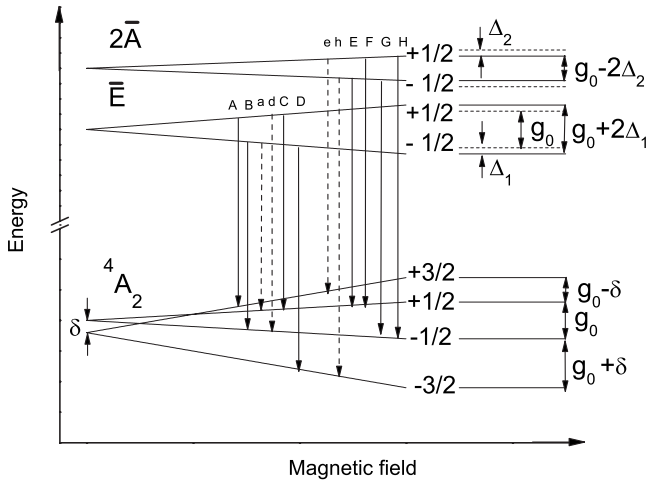

FIG. 5. Zeeman-splitting transitions diagram. Zero-field splitting (δ) is responsible for asymmetric 3/2 spin fourfold splitting of ground state. Intrinsic splitting of excited states (Δ_1) and (Δ_2) yields separation between $+1/2$ and $-1/2$ states to be observed in PL spectra. Arrows indicate emission transitions for allowed (solid lines) and forbidden (dashed line) transitions. Label characters identify these transitions in Figs. 3, 4, and 6.

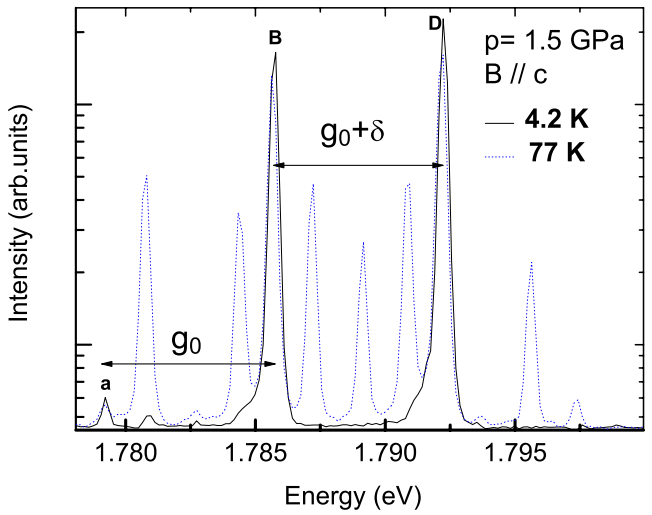

FIG. 6. (Color online) PL intensity spectrum (logarithmic scale) at maximum field (56 T) corresponding to Fig. 4 recorded at liquid-helium temperature. High-temperature spectrum is additionally plotted (dashed curve) to confirm peak assignation.

these three transitions (a,B,D) originate from this same level. Hence, the B line actually originates from the $(\bar{E}, -1/2)$ to $(^4A_2,-1/2)$ transition, whereas the C peak comes from the $(\bar{E},+1/2)$ to $(^4A_2,+1/2)$ transition. The origin of these lines seems to have been somehow misunderstood in the previous study of Hori *et al.*[17] based on high-field optical-absorption measurements maybe due to the absence of very low-temperature experiments. In addition, the very good signal-to-noise ratio and very strong magnetic field allow for the distinct observations of the lift of degeneracy between the Kramers' doublet states. Consequently, we have a direct measurement of the intrinsic splitting factors through the energy difference between B and C for Δ_1 on one hand and between F and G for Δ_2 on the other hand as it appears on Figs. 4 and 5.

2. Magnetic field applied perpendicular to the c axis

Considering hexagonal crystal symmetry of ruby, one can expect strong modifications of magnetic effects on spectra if the field is now applied perpendicularly to the optical axis c. Figure 7 presents the observed evolution of the magnetic splitting pattern recorded at 5.5 GPa, which is similar to ambient pressure reported experiments.[17,18] A clear Paschen-Back effect characterized by a nonlinear magnetic dependence of the emission lines energy is evidenced. One can notice the very good agreement of extreme line experimental points (M,U) with quadratic behavior fits (solid lines). Moreover, the evolution of the central energy R_{1M} and R_{2M} of R_1 and R_2 respective pattern is plotted in dashed lines. In fact, in this configuration, the two excited levels $\bar{E}$ and $2\bar{A}$ are mixed by a magnetic-driven interaction. The Cr^{3+} spin is originally aligned along the optical c axis because of a strong coupling with the trigonal distortion mediated by the spin-orbit interaction. However, if the magnetic field is strong enough, it tends to be completely quantized along the applied

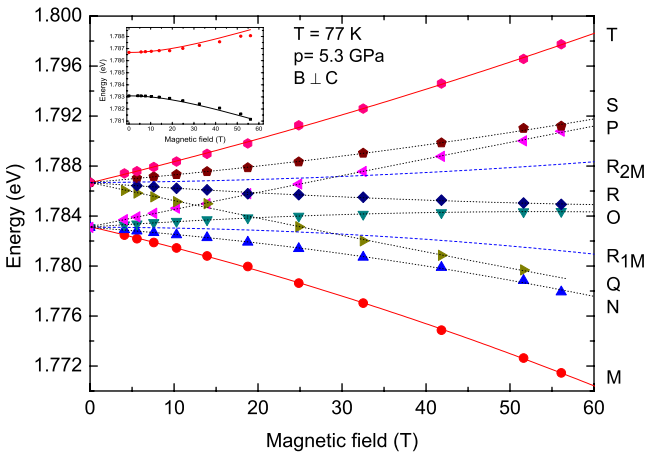

FIG. 7. (Color online) Magnetic shift pattern of ruby R lines with magnetic field perpendicular to the c axis. Experimental peak positions (symbols) are extracted from spectra recorded at different magnetic-field values after multi-Gaussian fits. Solid lines show a very good agreement with a magnetic quadratic behavior. Dashed lines (R_{1M},R_{2M}) are calculated central energies of the two R lines exhibiting clear quadratic repulsion between $\bar{E}$ and $2\bar{A}$ levels. Dotted lines are guides for the eyes. Inset presents a quadratic fit of this repulsion with Paschen-Back effect equation.

field. Therefore, taking energy scale origin between $\bar{E}$ and $2\bar{A}$, one obtains

$$E_{2\bar{A}} = \frac{1}{2}\sqrt{A^2 + (g_0\mu_B B)^2},$$

$$E_{\bar{E}} = -\frac{1}{2}\sqrt{A^2 + (g_0\mu_B B)^2}, \quad (2)$$

where A is the energy difference induced by anisotropy between $\bar{E}$ and $2\bar{A}$. The inset of Fig. 7 shows the good agreement obtained between R_{1M} and R_{2M} and quadratic fits assuming Eq. (2). The ratio between A and $g_0\mu_B B$ being equal to 2 at 60 T, the high-field regime is here experimentally achieved and explains the asymmetric behavior. Thus, the four peaks for each R line reflect only the $m_s = \pm 3/2$ ground-state linear Zeeman effect with isotropic constant g_0. The lift of degeneracy of the two Kramers' doublets is weak in this configuration and hidden by experimental linewidth. With the experimental FWHM of isolated P peak at liquid-helium temperature ($\sim 5.10^{-4}$ eV), we can only restrict $g_\perp$ to be smaller than 0.1.

An example of spectrum at 56 T and 4.2 K is shown in Fig. 8. The four peaks corresponding to the four Zeeman sublevels of the ground state are very well separated. We can extract ambient pressure values for $g_0 = 1.98$, which is consistent with both electron spin resonance (ESR) measurements[10] and our results with B along the c axis assuming that g_0 is isotropic.

B. Pressure dependence of Zeeman factors

After the comprehensive study of the magnetic effects on PL spectra at ambient pressure presented in Sec. III A, we

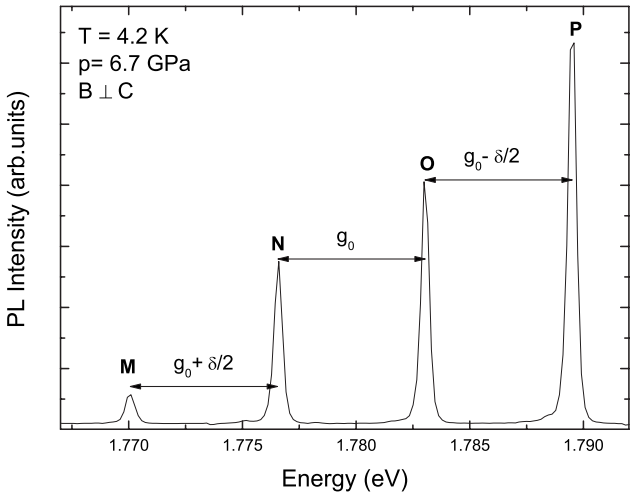

FIG. 8. PL spectrum of ruby at high pressure (6.7 GPa) and high magnetic field (56 T) recorded at 4.2 K in the Faraday configuration with B perpendicular to the c axis. Energy difference is given on arrows in $\mu_B B$ units according to peak assignment in Ref. 8.

have considered high-pressure effects. At first sight, no strong modification is observed but rigorous analysis of our precise data allowed getting important information on the electronic structure of chromium states in ruby under hydrostatic pressure up to 10 GPa.

The energy gap $A = E_{R_2} - E_{R_1}$ appears as a sensitive hydrostaticity probe as hydrostatic conditions are characterized by a very slight decrease up to 10 GPa, whereas pressure gradients induce large increase in the energy gap.[19] Our data exhibit such a slight decrease so we can assume that good hydrostaticity conditions are achieved in the compression chamber. Moreover, the full width at half maximum of the R_1 peak recorded at 77 K is only 40% wider at 10 GPa than at ambient pressure, which is also a good indication of hydrostaticity.

We have first paid a special attention to the possible modifications of g_0. Both configurations we used permit measurements of this parameter. Within experimental error, we can conclude that, in good agreement with previous optical and ESR studies under pressure, the ground-state Zeeman factor g_0 and the zero-field splitting parameter δ remain constant in the pressure range explored in our experiment.

Besides, we have studied the possible modification of the quadratic coefficient in the Paschen-Back pattern linked with the competition between anisotropy and applied field. However, the numerical quadratic parameters calculated through a pure parabolic numerical fit of the central energy (R_{1M},R_{2M}) of each R line are not modified. Thus the repulsion between the two excited states remains unchanged up to 6.7 GPa. These results for ruby differ from results obtained in alexandrite.[20] In this neighbor compound, the spin character is influenced by applied hydrostatic pressure and undergoes a progressive transition from a Heisenberg type, characterized by quasi-isotropic values of g parameters to an Ising type, where spin is quenched and aligned along one particular crystal axis. This is another evidence of good hydrostatic conditions in our setup considering that the A parameter is very sensitive to pressure gradients as demonstrated in Ref. 19.

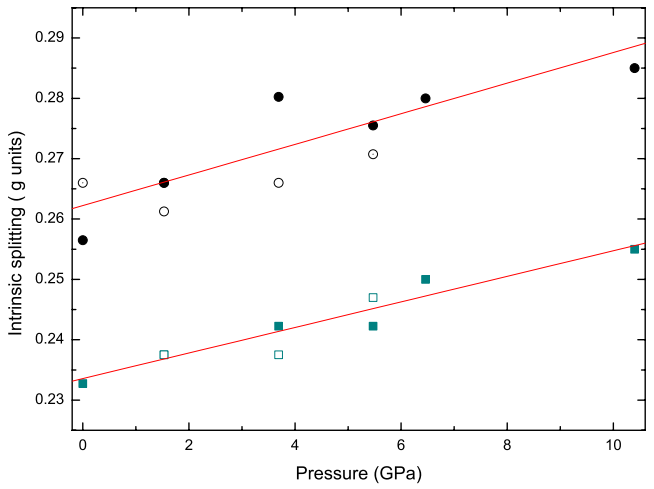

FIG. 9. (Color online) Pressure dependence of $2\bar{A}$ and $\bar{E}$ excited states intrinsic splitting factors Δ_1 (squares) and Δ_2 (dots). Filled symbols correspond to values calculated using the most intense peaks (B,C) and (F,G). Empty symbols come from weaker peaks. Linear shift is evidenced through the good agreement with linear fit (solid lines).

In addition, we have measured the pressure dependence of the low-temperature P peak FWHM up to 7 GPa. This width is strictly constant even at the highest achieved pressure. So, any possible pressure-induced enhancement of the perpendicular excited states splitting $g_\perp$ still remains below our experimental sensitivity with our current optical resolution and magnetic-field strength.

Furthermore, strong pressure dependence of the $\bar{E}$ and $2\bar{A}$ excited states' intrinsic Zeeman-splitting coefficient is evidenced on Fig. 9. Our values at 1 atm for Δ_1 and Δ_2, respectively, are 0.23 and 0.26 (in $\mu_B B$ units), in good agreement with reported values in Ref. 8. We have then analyzed the pressure evolution up to 10 GPa. Complete set of magneto-PL spectra has been recorded at six different values of the pressure. Our experimental data (filled symbols) are highly accurate as they are calculated from the energy differences between intense well-defined peaks (B,C) and (F,G). Besides additional information is extracted through weak peak $(a-h)$ energy analysis (empty symbols). These two sets of data are in remarkable accordance and appear in this way consistent. Both factors seems to be well described by, respectively, $0.23+(21\pm3)\times10^{-4}p$ and $0.26+(25\pm7)\times10^{-4}p$ where p is in GPa and the g factors are in units of $\mu_B B$. So, considering the uncertainty on these values we can assume a similar linear enhancement for both factors as follows:

$$\Delta_{\text{exp}} = 0.25 + 0.002p = 0.25(1 + 0.008p). \tag{3}$$

This result is in strong disagreement with behavior reported by Hori *et al.* in Ref. 1. However, this previous experimental study relies on only two different high-pressure values. Moreover, intrinsic splitting factors are indirectly extracted from the magnetic shift of very weak and spread absorption peaks owing to lack of optical resolution in this preliminary experiment.

The intrinsic splitting factors are due to a third-order interaction between $\bar{E}$ and $2\bar{A}$ states and upper excited states $^2F_1$ and $^2F_2$,

$$\Delta \sim \langle \bar{E}, 2\bar{A}|L_Z \times V_{\text{tr}} \times V_{\text{tr}}|^2F_1, {}^2F_2\rangle + \langle \bar{E}, 2\bar{A}|S_Z \times V_{\text{tr}} \times H_{\text{SO}}|^2F_1, {}^2F_2\rangle, \tag{4}$$

where L_Z and S_Z are the orbital and spin momenta along the c axis, V_{tr} is the trigonal field, and H_{SO} is the spin-orbit interaction Hamiltonian. One has to sum all the appropriate matrix elements suggested by this condensed form. Explicit expression could be found in Ref. 7. As $2\bar{A}$ is closer than $2\bar{E}$ to upper excited levels, the strength of the interaction is slightly larger and $\Delta_1 < \Delta_2$.

Nevertheless, the second term in Eq. (4) vanishes in our case and the remaining dominant term is

$$\Delta = 12K^2/[(E_R - E'_R)(E_R - E_B)], \tag{5}$$

where $K \sim \langle|V_{\text{tr}}|\rangle$ and E_R, E'_R, and E_B are, respectively, the mean energies of R, R', and B lines. Using the reported values by Eggert *et al.* in Ref. 21 for the pressure dependence of E_R, E'_R, and E_B, we find

$$K = \left[\frac{\Delta}{12}(E_R - E'_R)(E_R - E_B)\right]^{1/2} \propto [(1 + 0.008p)(1 - 9\times10^{-8}p)(1 - 8\times10^{-8}p)]^{1/2}. \tag{6}$$

Finally, the pressure dependence of Δ appears to control the evolution of the trigonal parameter K, with the two last term in Eq. (6) neglected at first order in p. Although, we can conclude that our experiments show an enhancement of the trigonal distortion in ruby crystal induced by hydrostatic compression. This structural rearrangement is consecutive to the volume reduction under pressure in this crystalline form, as the distortion tends to minimize repulsion between Cr^{3+} ions.[7,8]

IV. CONCLUSIONS

Magneto-optical measurements under high pressure have been successfully demonstrated on oriented ruby with our miniature diamond-anvil cell using 60 T pulsed magnetic fields. Better understanding of Zeeman lift of degeneracy of $\bar{E}$ and $2\bar{A}$ Kramers' doublet has been made possible. Moreover, a pressure-induced increase of the trigonal distortion parameter has been demonstrated by the observation of the variation in excited states Zeeman-splitting factors under pressure. Nevertheless, as the Paschen-Back splitting remains unchanged, no modification of the spin character is observed under compression in single crystals of ruby.

ACKNOWLEDGMENTS

The authors thank C. Power, J.-C. Chervin, B. Couzinet, and A. Polian for the DAC design; S. George for tailor-made

optical fiber luminescence probe; M. Jacquet and M. Escudier for sample preparation; and J.M. Poumirol for data analysis. The authors acknowledge M. Goiran, J. Leotin, H. Rakoto, S. Nanot, and B. Raquet for fruitful discussions. This work was supported in part by French PCP program "Nanotubes de Carbone" and by EuroMagNET under EU Contract No. RII3-CT-2004-506239. J.G. acknowledges support from the Ministerio de Educacion y Ciencia (Spain) under project MALTA-Consolider Ingenio 2010 (Contract No. CSD2007-00045).

*broto@lncmp.org
†Also at Centro de Estudio de Semiconductores, Universidad de Los Andes, Mérida, Venezuela.

[1] H. Hori, S. Endo, K. Yamamoto, H. Mikami, A. Yamagishi, and M. Date, Physica B (Amsterdam) **177**, 71 (1992).
[2] A. F. Bangura, P. A. Goddard, J. Singleton, S. W. Tozer, A. I. Coldea, A. Ardavan, R. D. McDonald, S. J. Blundell, and J. A. Schlueter, Phys. Rev. B **76**, 052510 (2007).
[3] H. Takahashi, K. Igawa, K. Arii, Y. Kamihara, M. Hirano, and H. Hosono, Nature (London) **453**, 376 (2008).
[4] J. Z. Cai, L. Lu, W. J. Kong, H. W. Zhu, C. Zhang, B. Q. Wei, D. H. Wu, and F. Liu, Phys. Rev. Lett. **97**, 026402 (2006).
[5] K. Yamamoto, S. Endo, and A. Yamagishi, Rev. Sci. Instrum. **62**, 2988 (1991).
[6] M. Nardone, A. Audouard, D. Vignolles, and L. Brossard, Cryogenics **41**, 175 (2001).
[7] S. Sugano and Y. Tanabe, J. Phys. Soc. Jpn. **13**, 880 (1958).
[8] S. Sugano and I. Tsujikawa, J. Phys. Soc. Jpn. **13**, 899 (1958).
[9] S. M. Sharma and Y. M. Gupta, Phys. Rev. B **43**, 879 (1991).
[10] H. Nelson, D. Larson, and H. Gardner, J. Chem. Phys. **47**, 1994 (1967).
[11] G. Piermarini, S. Blockand, J. Barnett, and R. Forman, J. Appl. Phys. **46**, 2774 (1975).
[12] A. Chijioke, W. Nellis, A. Soldatov, and I. Silvera, J. Appl. Phys. **98**, 114905 (2005).
[13] B. Weinstein, Rev. Sci. Instrum. **57**, 910 (1986).
[14] G. Piermarini, S. Blockland, and J. Barnett, J. Appl. Phys. **44**, 5377 (1973).
[15] J. Chervin, B. Canny, and M. Mancinelli, High Press. Res. **21**, 305 (2001).
[16] Q. Williams and R. Jeanloz, Phys. Rev. B **31**, 7449 (1985).
[17] H. Hori, H. Mollymoto, and M. Date, J. Phys. Soc. Jpn. **46**, 908 (1979).
[18] K. Aoyagi, A. Misu, and S. Sugano, J. Phys. Soc. Jpn. **18**, 1448 (1963).
[19] J. Besson and J. Pinceaux, Rev. Sci. Instrum. **50**, 541 (1979).
[20] N. Kuroda, H. Kanda, G. Kido, M. Takeda, Y. Nishina, and Y. Nakagawa, Jpn. J. Appl. Phys., Part 2 **31**, L700 (1992).
[21] J. Eggert, K. Goettel, and I. Silvera Phys. Rev. B **40**, 5724 (1989).